CHAPTER III

THEORY

3.1 Molecular Sieves for Use in Catalysis

The history of a new class of inorganic materials, zeolites and molecular sieves, has been reviewed from the finding of the first zeolite mineral in 1756 through the explosion in new molecular sieve structures and compositions in the 1980's [38]. Zeolites and molecular sieves are finding applications in many areas of catalysis, generating interest in these materials in industrial and academic laboratories [39-40]. As catalyst, zeolites exhibit appreciable acid activity with shape-selectivity features not available in the compositional equivalent amorphous catalysts. In addition, these materials can act as supports for numerous catalytically active metals. Major advances have occured in the synthesis of molecular sieve materials since the initial discovery of the synthetic zeolite molecular sieve's type A, X and Y, and a great number of techniques have evolved for identifying and characterizing these materials [38]. Added to extensive and ever growing list of aluminosilicate zeolites are molecular sieves containing other elemental compositions. These materials differ in their catalytic activity relative to the aluminosilicate zeolites and may have potential in being customized or tailored for specific applications. Elements isoelectronic with Al^{+3} or Si^{+4} have been proposed to be substituted into the framework lattice during synthesis. These included B^{+3}, Ga^{+3}, Fe^{+3}, and Cr^{+3} substituting for Al^{+3}, and Ge^{+4} and Ti^{+4} for Si^{+4}. The incorporation of

transition elements such as Fe^{+3} for framework Al^{+3} positions modifies the acid activity and, in addition, provides a novel means of obtaining high dispersions of these metals within the constrained pores of industrially interesting catalyst materials.

3.2 Classification of Molecular Sieves

With the recent discoveries of molecular sieve materials containing other elements in addition to, or in lieu of, silicon and aluminum, the casual interchange of the terms "molecular sieve" and "zeolite" must be reconsidered. In 1932 McBain [38] proposed the term "molecular sieve" to describe a class of materials that exhibited selective adsorption properties. He proposed that for a material to be a molecular sieve, it must separate components of a mixture on the basis of molecular size and shape differences. Two classes of molecular sieves were known when McBain put forth his definition: the zeolites and certain microporous charcoals. The list now includes the silicates, the metallosilicates, metalloaluminates, the $AlPO_4$'s, and silico- and metalloaluminophosphates, as well as the zeolites. The different classes of molecular sieve materials are listed in Figure 3.1 [40]. All are molecular sieves, as their regular framework structures will separate components of a mixture on the basis of size and shape. The difference lies not within the structure of these materials, as many are structurally analogous, but in their elemental composition. Therefore, all are molecular sieves though none but the aluminosilicates should carry the classical name, zeolite [40].
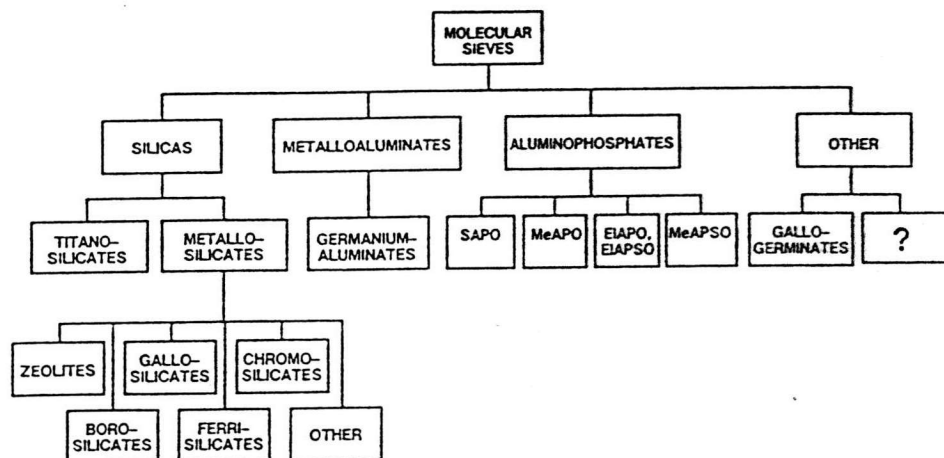
Figure 3.1 Classification of molecular sieve materials indicating extensive variation in composition. The zeolites occupy a subcategory of the metallosilicates [40].
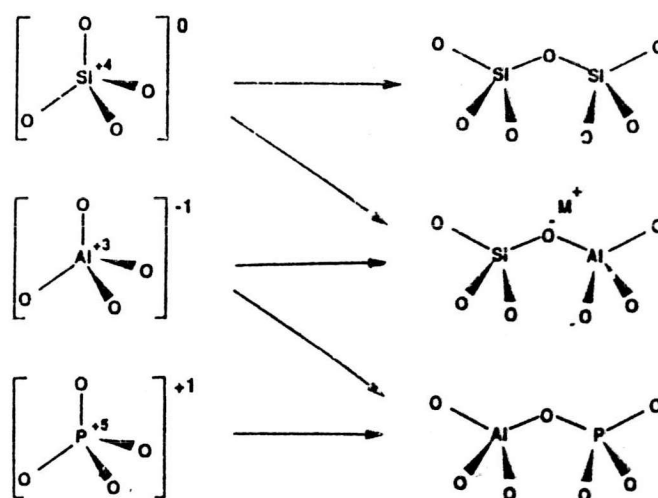

Figure 3.2 Basic building blocks of zeolites-molecular sieves [41].

3.2.1 Zeolites

Zeolites are crystalline aluminosilicate that are constructed from TO_4 tetrahedral (T= Tetrahedral atom , e.g. , Si, Al) ; each apical oxygen atom is shared with an adjacent tetrahedron [41]. Thus, the ratio of O/T is always equal to 2. A SiO_4 unit in framework (structure) is neutral since an oxygen bridges two T atoms and shares electron density with each other (Figure 3.2). However, since Al is +3, for every aluminum containing tetrahedron there is a net -1 charge which must be balanced by a cation. The tetrahedra are coordinated such that the zeolites have open framework structure with high surface areas. The framework thus obtained contains pores, channels, and cages, or interconnected voids. Access to the cavity is possible through voids of various sizes which are of the size of small molecules. Because of these unique properties, zeolites are able to be shape and size selective in catalytic molecular rearrangements [38].

Zeolites may be represented by the general formula,

$$M_{x/n} [(AlO_2)_x(SiO_2)_y]wH_2O$$
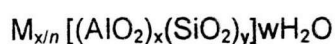
where the term in brackets is the crystallographic unit cell. The metal cation of valence n is present to produce electrical neutrality since for each aluminum tetrahedron in the lattice there is an overall charge of -1 [42]. M is a proton, the zeolite becomes a strong Bronsted acid, w is the number of water molecules per unit cell, and x, y are the total number of tetrahedra per unit cell [38].

Approximately 70 distinct structures of zeolites and molecular sieves are known [43]. There are natural zeolites, synthetic analogues of natural

zeolites, and synthetic zeolite with no natural counterparts. Their pore sizes range from 4 A^0 to 13 A^0. Zeolites with pores that are comprised of eight T-atoms (and eight oxygen atoms) are considered small pore zeolites. They have free diameters of 3.0-4.5 A^0 , e.g., zeolite A. Medium pore zeolites have pores formed by ten T-atom rings with 4.5-6.0 A^0 free diameter, e.g., ZSM-5. Zeolites with twelve or more T-atoms in rings that make up the pores are considered large pores zeolites. They have free diameters of 8.0 A^0 or more, e.g., zeolites X and Y[44]. To date, no zeolite (aluminosilicate) exists with pores larger than ~ 8 A^0 [41].

In type A zeolite, arge cavities are connected through apertures of 0.5 nm, determined by eight-membered rings (Figure 3.3a). The mordenite pore structure consists of elliptical and noninterconnected channels parallel to the c-axis of the orthorhombic structure. Their openings are limited by twelve-membered rings (0.6-0.7 nm) (Figure 3.3c) [42].

In silicalite and ZSM-5, the tetrahedra are linked to form the chain-type building block [40]. The chains can be connected to form a layer, as shown in Figure 3.4 [45]. Rings consisting of five O atoms are evident in this structure; the name pentasil is therefore used to describe it. Also evident in Figure 3.4 are rings consisting of 10 oxygen atoms; these are important because they provide openings in the structure large enough for passage of even rather large molecules. The layers can be linked in two ways; the neighboring layers being related either by the operation of a mirror or an inversion. The former pertains to the zeolite ZSM-11, the latter to silicalite or ZSM-5; the intermediate structures constitute the pentasil series.
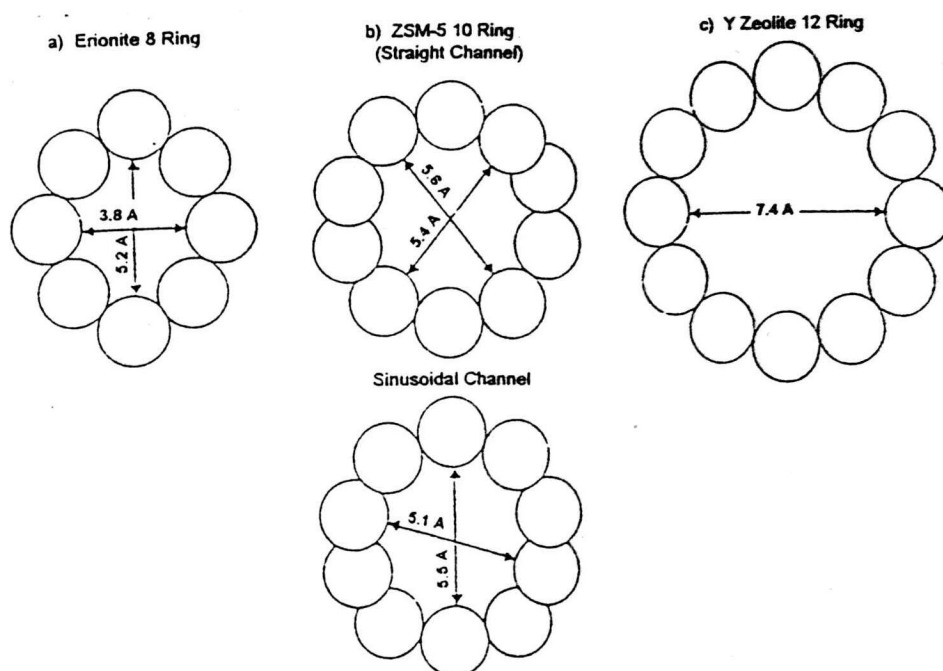
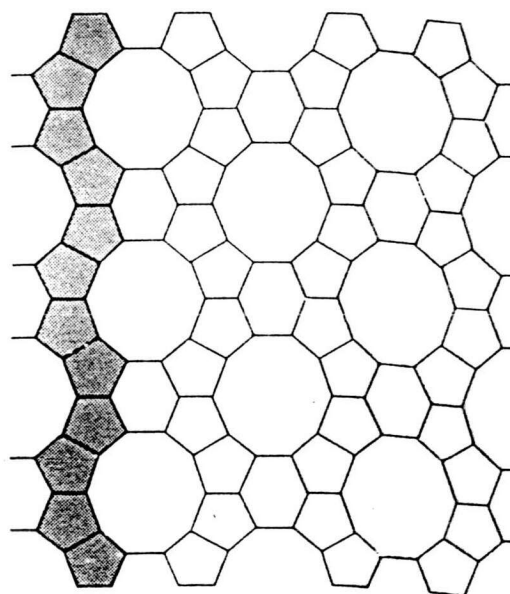Figure 3.3   Typical zeolite pore geometries [42].

Figure 3.4   Schematic diagram of silicalite layers, formed by linking of the chains

through sharing of oxygen in linked SiO_4 tetrahedra [45].

The three-dimensional structure of silicalite (and ZSM-5) is represented in Figure 3.5a [45]. The ten-membered rings (ca. 0.55 nm in diameter) (Figure 3.3b) provide access to a network of intersecting pores within the crystal. The pore structure consists of two intersecting channel systems as shown in Figure 3.5b: one straight and the other sinusoidal and perpendicular to the former [42]. Many molecules are small enough to penetrate into this intracrystalline pore structure, where they may be catalytically converted.

The properties of a zeolite depend on the structure of zeolite, the size of the free channels, the location, charge and size of the cation within the framework, the presence of faults and occluded material, and the ordering of T atoms (framework metal atoms). Therefore, structural information is important in understanding the adsorptive and catalytic properties of zeolites [46].

3.2.2 Non-aluminosilicate Molecular Sieves

The aluminosilicate zeolites offer the ion exchange properties, higher thermal stability, high acidity and shape-selective structural features desired by those working in the areas of adsorption and catalysis. However, modification and subsequent improvement of these properties have served as a driving force for changing the composition of these microporous materials [40].

Advances in the area of new molecular sieve materials have come in the preparation of zeolite-like structure containing framework components other than aluminum and silicon exclusively. There are now many non-aluminosilicate molecular sieves [46]. Referring to Figure 3.2, if tetrahedra containing aluminum and phosphorous, which is aluminophosphate or $AlPO_4$, are connected in a strict $Al/P = 1$, a neutral framework is obtained. Also, other
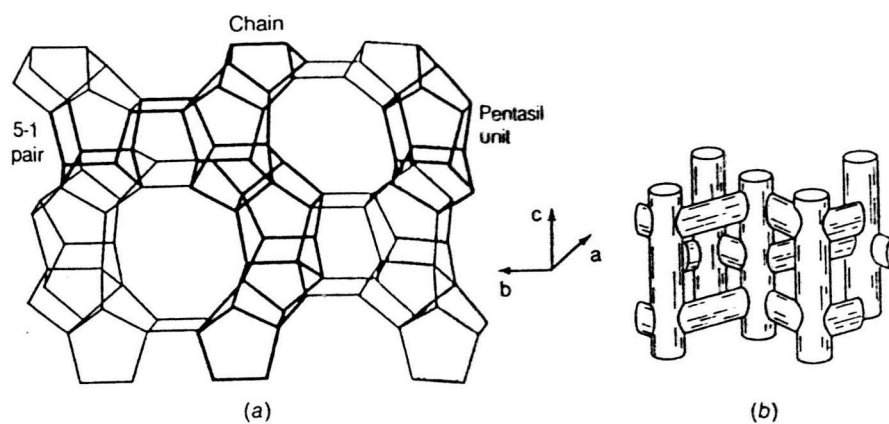
Figure 3.5 Three-dimensional structure of silicalite (ZSM-5) [45].

(a) Structure formed by stacking of sequences of layers.
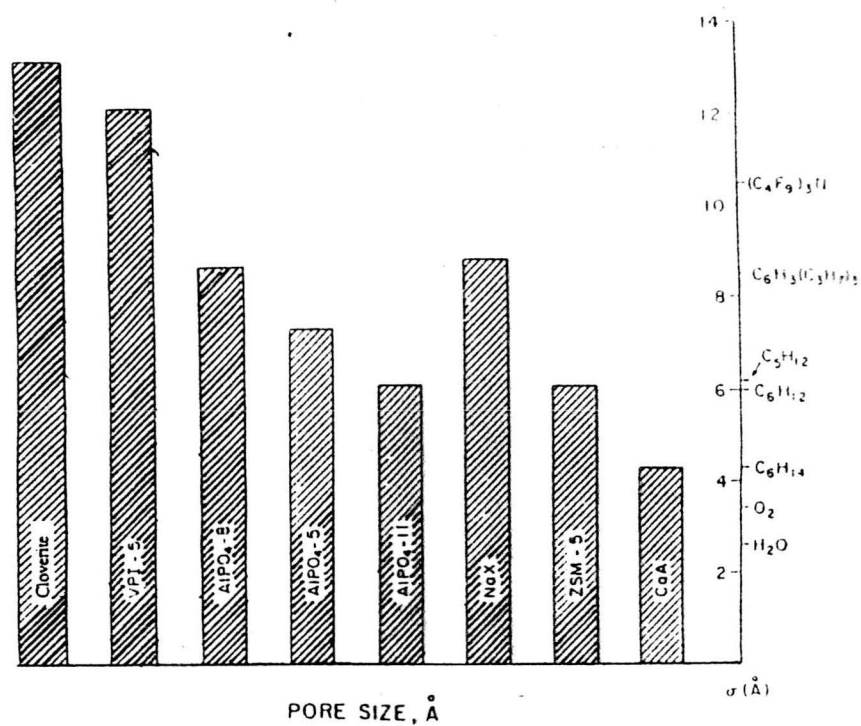
(b) Channel network.

Figure 3.6 Typical zeolites pore sizes compared to the diameter of various

molecules[46].

elements can be incorporated into the $AlPO_4$ framework to make them charged, e.g., silicoaluminophosphates or SAPO's. Phosphate-based molecular sieves have extended the pore size range from 8 A^0 to 13 A^0. Figure 3.6 shows some typical framework projections containing various rings (pores) of different sizes. However, it should be noted that the data shown for cloverite and $AlPO_4$-8 are the maximum dimension as determined from the crystal structure. For $AlPO_4$-8 , the structure is faulted and the adsorption behavior that would be expected from the crystal structure cannot be obtained [46]. Also, adsorption data revealing the size of cloverite is not yet reported [46].

3.3 Acidity of Zeolite

Classical Bronsted and Lewis acid models of acidity have been used to classify the active sites on zeolites. Bronsted acidity is proton donor acidity; a trigonally co-ordinated alumina atom is an electron deficient and can accept an electron pair, therefore behaves as a Lewis acid [47,48].

In general, the increase in Si/Al ratio will increase acidic strength and thermal stability of zeolite [49]. Since the number of acidic OH groups depend on the number of aluminum in zeolite's framework, decrease in Al content is expected to reduce catalytic activity of zeolite.

Based on electrostatic consideration, the charge density at a cation site increases with increasing Si/Al ratio. It was conceived that this phenomenon is related to the reduction of electrostatic interaction between framework sites, and possibly to the difference in the order of aluminum in zeolite crystal [48].

Recently it has been reported the mean charge on the proton was shifted regularly towards higher values as the Al content decreased [47]. Simultaneously the total number of acidic hydroxyls, governed by the Al atoms, were decreased. This evidence emphasized that the entire acid strength distribution (weak, medium, strong) was shifted towards stronger values. That is, weaker acid sites become stronger with the decrease in Al content.

An improvement in thermal or hydrothermal stability has been ascribed to the lower density of hydroxyls groups which parallel to that of Al content [42]. A longer distance between hydroxyl groups decreases the probability of dehydroxylation that generates defects on structure of zeolites.

3.4 Generation of Acid Centers

Protonic acid centers of zeolite are generated in various ways. Figure 3.7 depicts the thermal decomposition of ammonium exchanged zeolites yielding the hydrogen form [40].

The Bronsted acidity due to water ionization on polyvalent cations, described below, is depicted in Figure 3.8 [42].

$$Mn^+ + xH_2O \longrightarrow M(OH)_x^{(n-x)+} + xH^+ \tag{3.1}$$
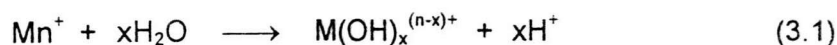
The exchange of monovalent ions by polyvalent cations could improve the catalytic property. Those highly charged cations create very acidic centers by hydrolysis phenomenon.
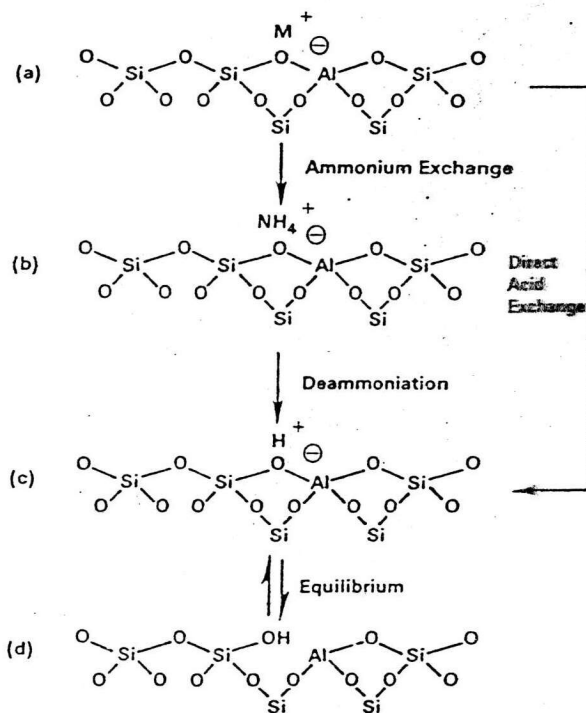
Figure 3.7 Diagram of the surface of zeolite framework [40].

(a) In the as-synthesized form M^{+1} is either an organic cation
or an alkalimetal cation.

(b) Ammonium in exchange produces the NH_4^+ exchanged form.

(c) Thermal treatment is used to remove ammonia, producing the H^{+1}
acid form.

(d) The acid form in (c) is in equilibrium with the form shown in (d),
where there is a silanol group adjacent to a tricoordinate aluminum.
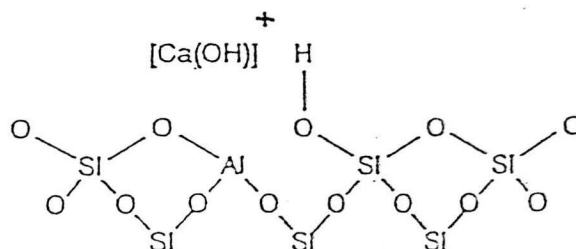
Figure 3.8 Water molecules coordinated to polyvalent cation are dissociated by heat treatment yielding Bronsted acidity [42].
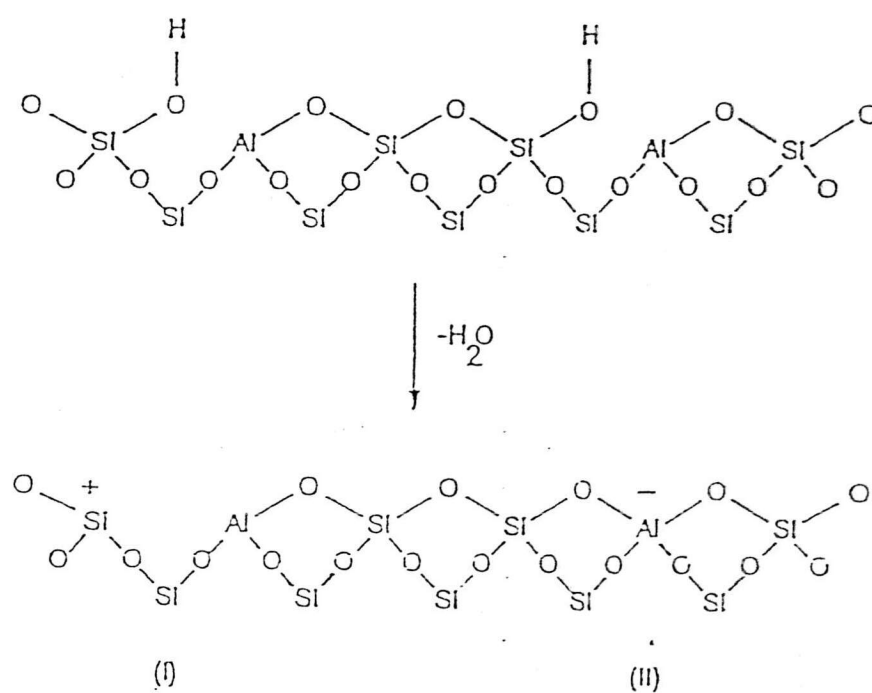

Figure 3.9 Lewis acid site developed by dehydroxylation of Bronsted acid site [42].

Bronsted acid sites are also generated by the reduction of transition metal cations. The concentration of OH groups of zeolite containing transition metals was noted to increase by reduction with hydrogen at 250-450 °C and to increase with the rise of the reduction temperature [42].

$$Cu^{2+} + H_2 \longrightarrow Cu^0 + 2H^+ \qquad (3.2)$$

$$Ag^+ + 1/2H_2 \longrightarrow Ag^0 + H^+ \qquad (3.3)$$
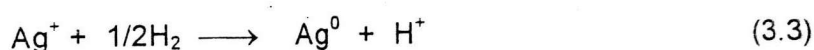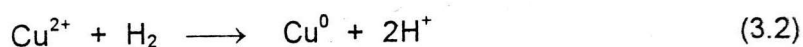
The formation of Lewis acidity from Bronsted sites is depicted in Figure 3.9 [42]. The dehydration reaction decreases the number of protons and increases that of Lewis sites.

Bronsted (OH) and Lewis (Al) sites can be present simultaneously in the structure of zeolite at high temperature. Dehydroxylation is thought to occur in ZSM-5 zeolite above 500 °C and calcination at 800 to 900 °C produces irreversible dehydroxylation which causes defection in crystal structure of zeolite.

Dealumination is believed to occur during dehydroxylation which may result from the steam generation within the sample [42]. The dealumination is indicated by an increase in the surface concentration of aluminum on the crystal. The dealumination process is expressed in Figure 3.10 [42]. The extent of dealumination monotonously increases with the partial pressure of steam.

The enhancement of the acid strength of OH groups is recently proposed to be pertinent to their interaction with those aluminum species sites and are tentatively expressed in Figure 3.11 [42]. Partial dealumination might,
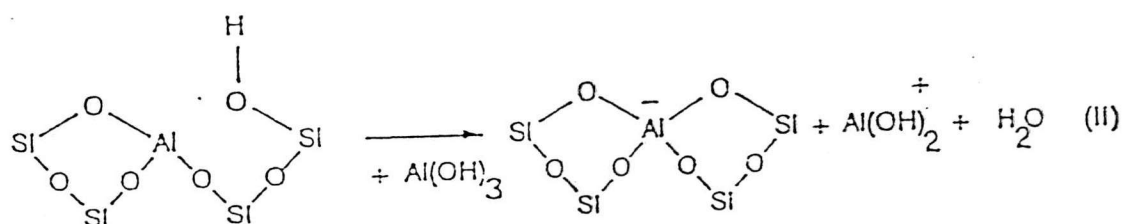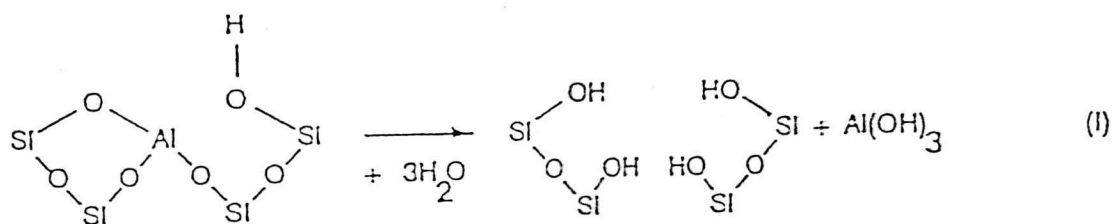
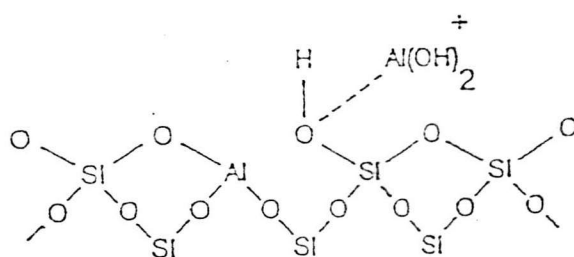Figure 3.10 Steam dealumination process in zeolite [42].

Figure 3.11 The enhancement of the acid strength of OH groups by their

interaction with dislodged aluminum species [42].

therefore, yield a catalyst of higher activity while severe steaming reduces the catalytic activity.
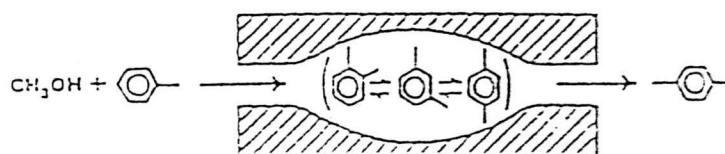
3.5 Shape Selectivity

There are several types of shape and size selectivity in zeolites. Firstly, reactant or charge selectivity results from the limited diffusibility of some of reactants, which cannot effectively enter and diffuse inside crystal pore structures of the zeolites. A particularly good illustration of this behavior is given by Weisz and co-workers [50]. Zeolites A and X were ion exchanged with calcium salts to create acid sites within the zeolite. These acid sites are formed as the water of hydration around the calcium ions hydrolyzes. When these zeolites are contacted with primary and secondary alcohols in the vapor phase, both alcohols dehydrate on CaX but only the primary one reacts on CaA. Since the secondary alcohol is too large to diffuse through the pores of CaA, it cannot reach the active sites within the CaA crystals. This kind of selectivity is called reactant shape selectivity and is illustrated in Figure 3.12 (a).

Product shape selectivity occurs when reaction products of different sizes are formed within the interior of the zeolite crystals and some of the products formed are too bulky to diffuse out [51]. The products which cannot escape from the cavities may undergo secondary reactions to smaller molecules or may deactivate the catalyst by blocking pores. A classic example of this type of selectivity is the monomolecular isomerization reactions of alkylaromatics as depicted in Figure 3.12 (b). The diffusion coefficient for para-xylene in ZSM-5 is approximately a thousand times that of either ortho or meta-xylene. Hence, essentially pure para-xylene is observed leaving the zeolite. Direct evidence for

a) Reactant selectivity
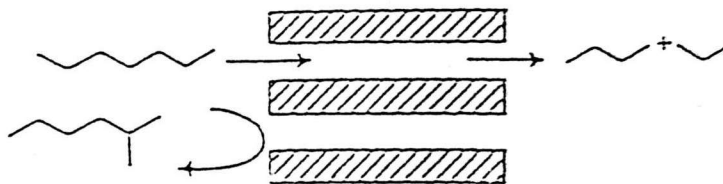
b) Product selectivity

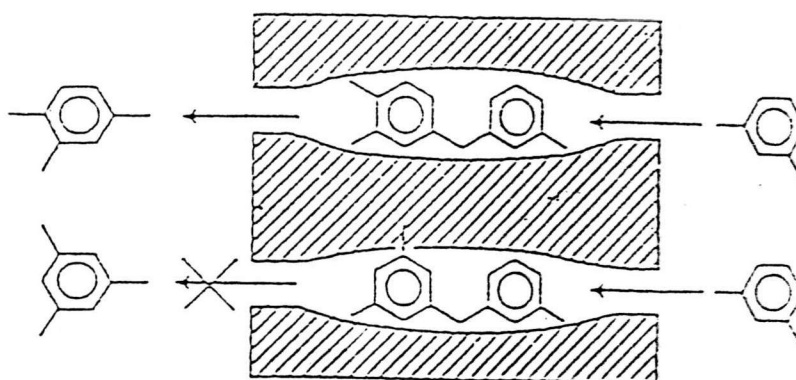c) Transient state selectivity

Figure 3.12 Schematic representation of the types of shape selectivity exhibited

by zeolites [50].

this type of shape selectivity has been reported by Anderson and Klinowski [52] for the catalytic conversion of methanol to hydrocarbons in ZSM-5. During the reaction, methanol is dehydrated to dimethyl ether (DME). The equilibrium mixture between methanol and DME reacts to form olefins, aliphatics and aromatics. By using in situ magic angle spinning NMR, 29 different organic species were identified in the adsorbed phase; however not all of these were observed with gas chromatography. For example, the tetramethylbenzenes that are formed in the pores of ZSM-5 do not diffuse out from the zeolites to be observed with gas chromatography.

Another type of shape selectivity is transition-state shape selectivity. For this type of selectivity, certain types of transition-state intermediates are too large to be accommodated within the pores/cavities of the zeolites. However, neither the reactants or the products are restricted from diffusing through the pores of zeolites. A good example of this type of selectivity is the transalkylation of dialkylbenzenes. In this reaction, an alkyl group is transferred from one molecule to another through a diphenylmethane transition state. For meta-xylene, this reaction will produce 1,3,5- as well as 1,2,4-trialkylbenzene. However, the transition state for the reaction that yields 1,3,5-trialkylbenzene is too large to be accommodated within the pores of mordenite. Consequently, only 1,2,4-trialkylbenzene is selectively formed inside the zeolite as illustrated in Figure 3.12 (c).

The critical diameter (as opposed to the length) of the molecules and the pore channel diameter of zeolites are important in predicting shape selective effects. However, molecules are deformable and can pass through opening

which are smaller than their critical diameters . Hence, not only size but also the dynamics and structure of the molecules must be taken into account.

Table 3.1 [53] presents values of selected critical molecular diameters and Table 3.2 [40] presents value of the effective pore size of various zeolites correlation between pore size of zeolites and kinetic diameter of some molecules are depicted in Figure 3.13 [54]

3.6 Reduction of NO_x

A major source of nitric oxide emission is fuel combustion in engines and power plants [55]. NO_x emissions also can be significant in chemical operations such as nitric acid plants. More recently, the emissions of nitrous oxides (N_2O) from fiber production plants have received attention because of its global warming effects. The nitric oxide and SO_x emissions are components of acid rain since, when mixed with water vapor in the clouds, they form nitric and sulfuric acid, respectively. Furthermore, NO_x participates in photochemical ozone (smog) generation by reaction with hydrocarbons.

3.6.1 Nonselective Catalytic Reduction of NO_x

One of the earliest techniques used to abate NO_x emissions from engines and nitric acid plants was to deplete the oxygen by operating the engine near stoichiometric or by adding a hydrocarbon or purge gas to deplete the oxygen via a chemical reaction in the exhaust [55].
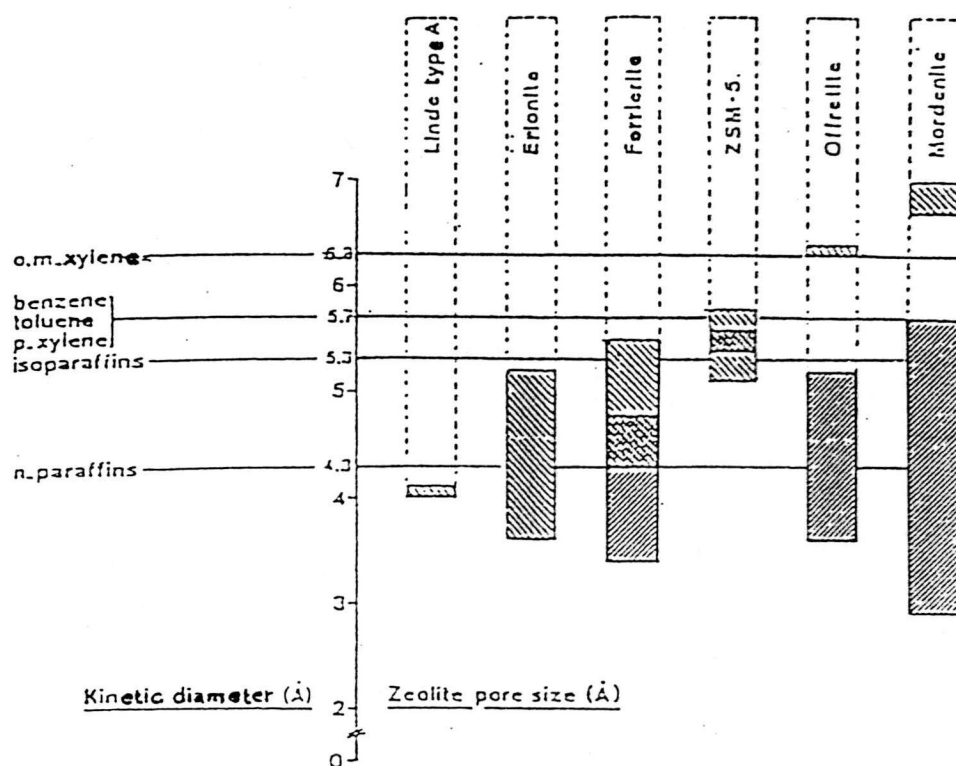
Figure 3.13 Correlation between pore size(s) of various zeolites and kinetic diameter of some molecules [54].

Table 3.1 Kinetic diameters of various molecules based on the Leonard-Jones relationship [53].

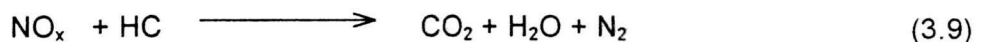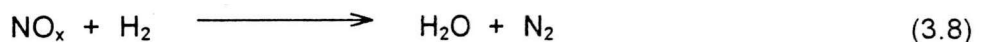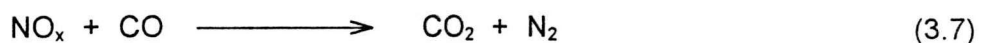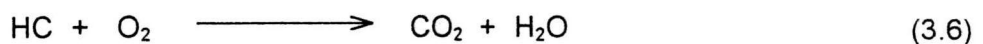|	KINETIC DIAMETER (ANGSTROMS)
He	2.6
H_2	2.89
O_2	3.46
N_2	3.64
NO	3.17
CO	3.76
CO_2	3.3
H_2O	2.65
NH_3	2.6
CH_4	3.8
C_2H_2	3.3
C_2H_4	3.9
C_3H_8	4.3
$n\text{-}C_4H_{10}$	4.3
Cyclopropane	4.23
$i\text{-}C_4H_{10}$	5.0
SF_6	5.5
Neopentane	6.2
$(C_4F_9)_3N$	10.2
Benzene	5.85
Cyclohexane	6.0

Table 3.2 Shape of the pore mouth opening of known zeolite structures. The dimensions are based on two parameters, the T atom forming the channel opening (8, 10, 12 rings) and the crystallographic free diameters of the channels. The channels are parallel to the crystallographic axis shown in brackets (e.g. <100>) [40].

STRUCTURE	8-MEMBER RING	10-MEMBER RING	12-MEMBER RING
Bikitaite	3.2×4.9[001]		
Brewsterite	2.3×5.0[100]		
	2.7×4.1[001]		
Cancrinite			6.2[001]
Chabazite	3.6×3.7[001]		
Dachiardite	3.6×4.8[001]	3.7×6.7[010]	
TMA-E	3.7×4.8[001]		
Edingtonite	3.5×3.9[110]		
Epistilbite	3.7×4.4[001]	3.2×5.3[100]	
Erionite	3.6×5.2[001]		
Faujasite			7.4<111>
Ferrierite	3.4×4.8[010]	4.3×5.5[001]	
Gismondine	3.1×4.4[100]		
	2.8×4.9[010]		
Gmelinite	3.6×3.9[001]		7.0[001]
Heulandite	4.0×5.5[100]	4.4×7.2[001]	
	4.1×4.7[001]		
ZK-5	3.9<100>		
Laumontite		4.0×5.6[100]	
Levyne	3.3×5.3[001]		
Type A	4.1<100>		
Type L			7.1[001]
Mazzite			7.4[001]
ZSM-11		5.1×5.5[100]	
Merlinoite	3.1×3.5[100]		
	3.5×3.5[010]		
	3.4×5.1[001]		
	3.3×3.3[001]		
ZSM-5		5.4×5.6[010]	
		5.1×5.5[100]	
Mordenite	2.9×5.7[010]		6.7×7.0[001]
Natrolite	2.6×3.9<101>		
Offretite	3.6×5.2[001]		6.4[001]
Paulingite	3.9<100>		
Phillipsite	4.2×4.4[100]		
	2.8×4.8[010]		
	3.3[001]		

For stationary engine operation, the engine is normally operated near stoichiometric conditions, whereby the catalytic chemistry is very similar to automotive three-way catalyst technology. A typical response of engine emissions from a natural gas fired stationary engine is given in Figure 3.14 [55].

The main differences from this application relative to automotive exhaust control are in the operating conditions (temperature, steady-state operation, and so forth) and the aging phenomenon. A typical application of engine nonselective catalytic reduction (NSCR) of NO_x would be the natural gas recompression engines used on gas pipelines throughout the Unites States or for small co-generation engines in hospitals, universities, and other institutions. The NO_x, CO, and sometimes HC emissions are to be controlled. In situation where high conversions are required, the engine will be epuipped with feedback control loop to maintain the engine operation near stoichiometric. Also, a second catalyst may be added with air injection to further reduce CO and HC emissions [55].

The major reaction involved NSCR NO_x are as follows:

$$CO + 1/2\,O_2 \longrightarrow CO_2 \tag{3.4}$$

$$H_2 + 1/2\,O_2 \longrightarrow H_2O \tag{3.5}$$

$$HC + O_2 \longrightarrow CO_2 + H_2O \tag{3.6}$$

$$NO_x + CO \longrightarrow CO_2 + N_2 \tag{3.7}$$

$$NO_x + H_2 \longrightarrow H_2O + N_2 \tag{3.8}$$

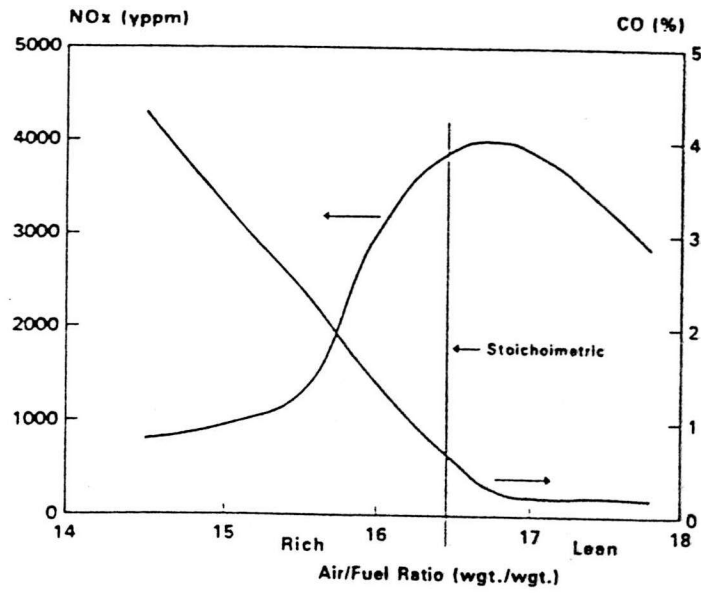$$NO_x + HC \longrightarrow CO_2 + H_2O + N_2 \tag{3.9}$$

Figure 3.14   Emissions of natural gas fueled stationary engine as a function of air-to-fuel ratio [55].
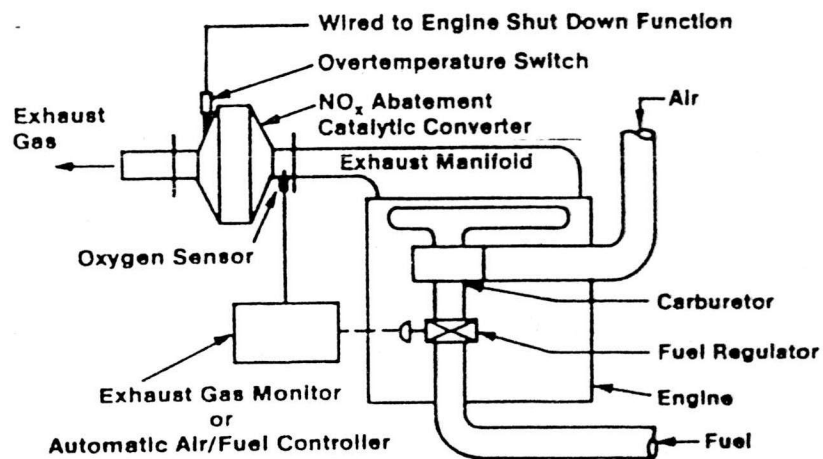

Figure 3.15   Major equipment in NSCR system for stationary engines [55].

A typical commercial catalyst ranges from 0.1 to 0.5 percent platinum, plus rhodium supported on a high surface area γ-Al_2O_3 washcoated onto a 200 to 400 cells per square inch (cpsi) ceramic honeycomb. There are, however, limited cases where beaded catalyst beds of similar catalyst compositions are in operation. Usually, the reactor operates at 50,000 hr^{-1} to 100,000 hr^{-1} space velocity. A schematic of an NSCR NO_x system for engines is given in Figure 3.15 [55]. The performance of an NSCR NO_x catalyst for a given engine operating condition is shown in Figure 3.16 [56]. The operating temperatures range from 450 to 900 $^\circ$C, with the co-generation applications having the higher range. Thermal deactivation is rare but does occur, mainly through engine maladjustments or some failure mode such as miss-fueling (e.g. bad fuel injector), misfire (e.g., bad spark plug), and so on [56]. Normal operating conditions are well within the range for the stability of the catalytic elements of Pt and Rh and the components used to stabilize the surface area. The major mode of the deactivation is masking of the catalyst with materials from the engine (e.g., lubricating oil, turbocharger coolant, etc.) [56].

The other major application of NSCR technology is in the abatement of the exhaust gas from nitric acid plants. This so-called tail gas abatement is one of the earliest techniques to abate NO_x emissions from oxidizing environments. Nitric oxide emission produced during the manufacture of nitric acid by high-temperature catalytic oxidation of NH_3 can be conveniently abated by a nonselective process [57]. Reddish-brown NO_2 is emitted into the atmosphere in the presence of excess air. Since the environment is oxidizing , and NO_2 must be reduced to N_2, it is necessary in NSCR to first consume all the excess O_2 by combustion by adding a fuel such as CH_4 (natural gas), LPG, or purge gas. The
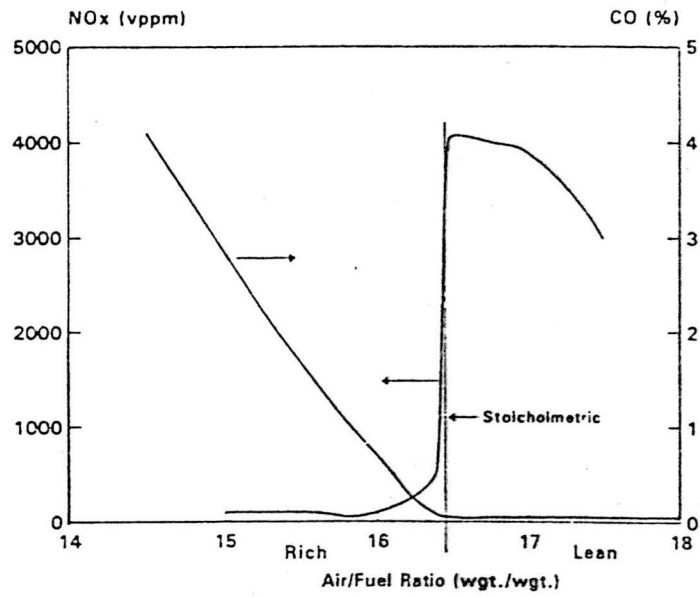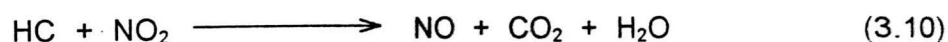
Figure 3.16   Emissions of natural gas fueled stationary engine with an NSCR system [56].

NO_2 is then catalytically reduced to N_2 by the residual fuel or its by-products (i.e., CH_4, CO, and so on). Tail gas abatement is accomplished through a three-step process as shown by the following reactions [57]:

$$HC + NO_2 \longrightarrow NO + CO_2 + H_2O \qquad (3.10)$$

As evidence from the reddish-brown plume, the tail gas contains predominantly NO_2. In fact, in the 1960s, this was the only reaction used. The effluent was bleached or visibly clear, and the NO was diluted quickly so that the visible color on reoxidation in the ambient air went unnoticed.
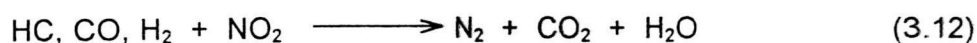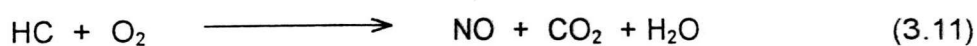
$$HC + O_2 \longrightarrow NO + CO_2 + H_2O \qquad (3.11)$$
$$HC, CO, H_2 + NO_2 \longrightarrow N_2 + CO_2 + H_2O \qquad (3.12)$$
$$\text{(NO reduction)}$$

The catalyst ranges from 0.3 to 0.5 percent by wt. platinum, plus small amounts of rhodium deposited on an alumina carrier upon a ceramic honeycomb structure. Again, in some instances, a beaded catalyst is used [57]. The operating temperature varies, depending on the fuel used to deplete the oxygen. Purge gas, which contains some H_2 and CO, operates at 300-350 °C, while natural gas requires a higher temperature of 500-550 °C. LPG usually requires 350-450 °C. Normally, these reactors operate at 50,000 to 100,000 hr^{-1} space velocity.

Deactivation usually occurs because of thermal sintering of the precious metal and/or Al_2O_3 after continuous exposure to temperatures near 900°C

caused by the exothermic nature of the process [57]. Deposition of iron from upstream corrosion of piping can also deactivate the catalyst. Phosphorous from the compressor lubricating oils is also a common poison that masks the catalytic sites.

3.6.2 Selective Catalytic Reduction of NO_x

3.6.2.1 The Reduction of NO_x Using Ammonia

Selective catalytic reduction (SCR) of NO_x using NH_3 was first discovered in 1957 [7]. It was discovered that NH_3 can react selectively with NO_x, producing elemental N_2 over a Pt catalyst in excess amount of oxygen. The major desired reactions are:

$$4NH_3 + 4NO + O_2 \longrightarrow 4N_2 + 6H_2O \qquad (3.13)$$

$$4NH_3 + 2NO_2 + O_2 \longrightarrow 3N_2 + 6H_2O \qquad (3.14)$$

One undesirable reaction produces N_2O which, given its strong infrared absorptivity, is considered to be a powerful greenhouse gas:

$$2NH_3 + 2O_2 \longrightarrow N_2O + 3H_2O \qquad (3.15)$$

At temperature below about 100-200 °C, the ammonia can also react with the NO_2 present in the process gas producing explosive NH_4NO_3 [57].

$$2NH_3 + 2NO_2 + H_2O \longrightarrow NH_4NO_3 + NH_4NO_2 \qquad (3.16)$$
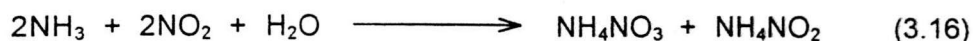
This reaction can be avoided by never allowing the temperature to fall below about 200 °C. The tendency for formation of NH_4NO_3 can also be minimized by metering into the gas stream less than the precise amount of NH_3 mecessary to react stoichiometrically with the NO_x (1 to 1 mole ratio) [55]. By doing so, there is little excess NH_3 that can "slip" out of the reactor.

As examples of the responses of an SCR catalyst to temperature and NH_3/NO_x feed conditions, Figures 3.17 and 3.18 demonstrate the NO_x conversion and NH_3 slip as a function of the NH_3/NO_x ratio and temperature for a V_2O_5/TiO_2 monolithic catalyst [57].

It is apparent that NH_3/NO_x ratios much greater than 1 result in significant NH_3 slip. In all applications, there is always a specification on permitted NH_3 slip. Frequently, this is < 5-10 vppm [57]. The major reactions involved in SCR NO_x reduction are depicted schematically in Figure 3.19 [57].

When sulfur is present in the flue gas, such as in coal-fired boilers or power plants, or in petroleum-derived liquid fuels such as distillate or diesel, the oxidation of SO_2 to SO_3 results in formation of H_2SO_4 upon reaction with H_2O [57]. Obviously, this results in condensation downstream and excessive corrosion of process equipment.

$$2SO_2 + O_2 \longrightarrow 2SO_3 \qquad (3.17)$$

$$SO_3 + H_2O \longrightarrow H_2SO_4 \qquad (3.18)$$

Few applications of SCR NO_x catalysts existed until the early 1970s, when reductions of the emission of NO_x became an important control issue for stationary power sources in Japan [57]. The Pt technology was not applicable
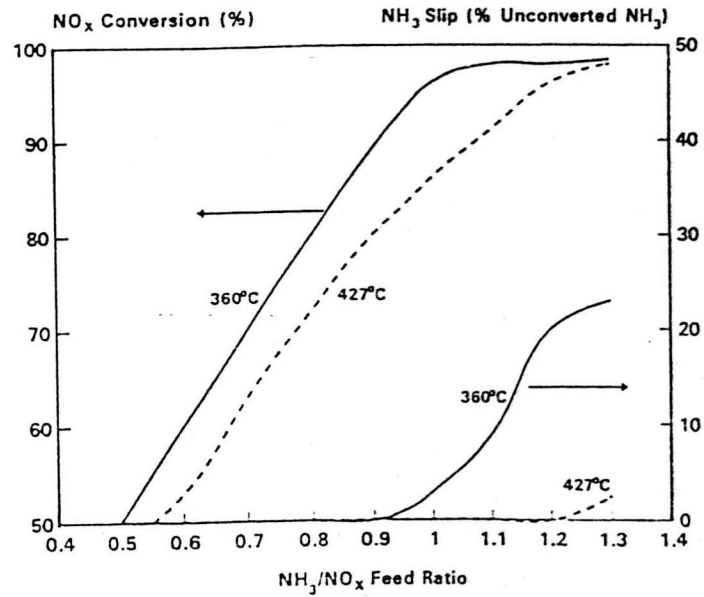
Figure 3.17   Effect of NH₃/NOₓ feed ratio on NOₓ conversion and NH₃ slip for V₂O₅/TiO₂ SCR catalyst on 2000 cpsi [57].
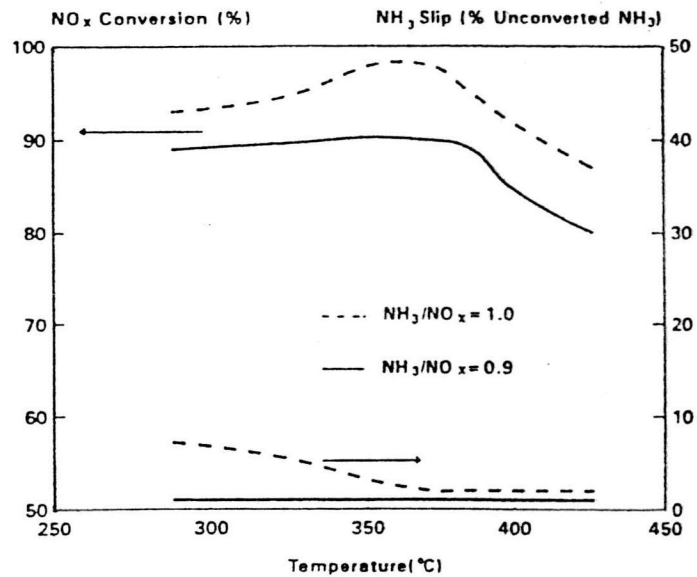

Figure 3.18   Effect of temperature on NOₓ conversion and NH₃ slip for V₂O₅/TiO₂ SCR catalyst on 2000 cpsi [57].
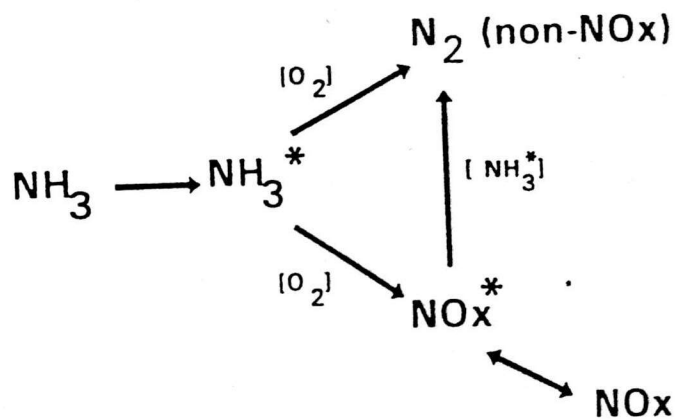
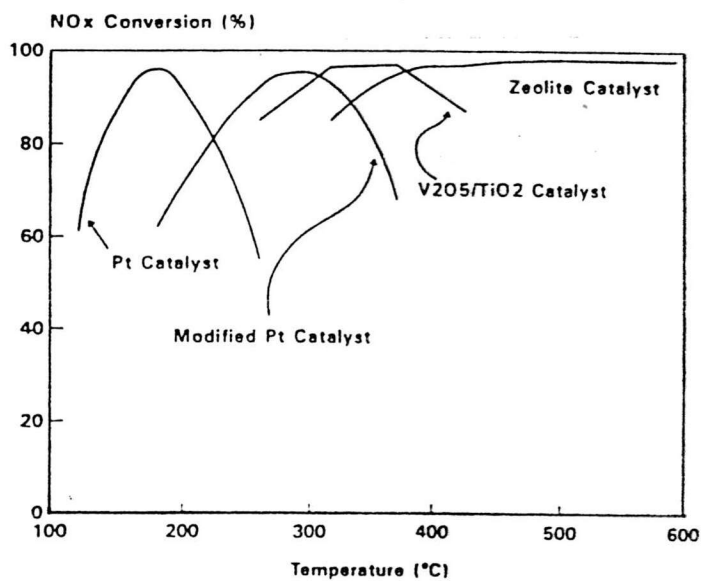Figure 3.19   Reaction network-catalytic reaction scheme of NH_3, NO_x, and O_2 [57].

Figure 3.20 Operation temperature windows for different SCR catalyst

formulations [57].

in this exhaust temperature region (i.e.,>250°C) becauce of its poor selectivity for NO_x reduction at these higher temperatures. Thus, it was during this period that the base metal catalysts were invented. Figure 3.20 [57] shows a comparison of the operating temperature range for the various catalyst technologies available for SCR NO_x. Note that the Pt catalysts lose selectivity above 250°C. At > 250°C, V_2O_5/Al_2O_3 was used first. However, it was restricted to sulfur-free exhaust gases because the alumina reacted with SO_3 to form $Al_2(SO_4)_3$ and deactivated the catalyst. This problem led to another key development, the use of a nonsulfating TiO_2 carrier for the V_2O_5, which then became the catalyst of choice. These catalysts functioned at higher temperatures and over a broader range than Pt.

Finally, quite recently, zeolite based catalysts have been developed that function at higher temperatures [57].

SCR catalysts can be prepared in a number of different geometric structures [57]. Some are extruded into pellets or homogeneous monoliths, while others are supported on parallel metal plates or ceramic honeycomb structures, and still others are fixed on a wire mesh. The appropriate structure depends on the end-use application.

Since each general class of catalyst material has different temperature performance characteristics, the engineer has considerable design flexibility to select the most cost-effective catalyst composition, structure, and operating system to optimize the abatement process. The active catalytic component and temperature ranges may be classified as indicated below [57] :

* Low temperature (175-250°C) : platinum

* Medium temperature (300-450°C) : vanadium

* High temperature (350-600°C) : zeolite

A more complete list of catalyst manufactureres, general catalyst compositions, catalyst support structures, and temperatures of operation is shown in Table 3.3 [57].

3.6.2.2 The Reduction of NO_x Using Hydrocarbons

There is a great incentive to use natural gas or other hydrocarbons as a reductant in stationary SCR rather than NH_3 [57].

$$CH_4 + 2NO_x + O_2 \longrightarrow N_2 + 2H_2O + CO_2 \qquad (3.19)$$

For many new power plants, natural gas is commonly used as a fuel and is readily available. Secondly, NH_3 is more expensive, requires special handling and storage, and requires a sophisticated metering system to avoid NH_3 slip. Technology referred to as lean NO_x is in the early stage of development [57]. The modern three-way catalytic converter (TWC) is efficient in the simultaneous reduction of CO, HC and NO_x [1]. A requirement for automotive three way catalyst is that the air-to-fuel combustion ratio be at the stoichiometric point, which for gasoline engine is 14.6 on a weight basis. Leaner ratios greater than 14.6 would result in a decrease in fuel consumption, but the TWC cannot reduce NO_x in this condition. Thus, the challenge is clear: develop a catalytic system for a lean-burn engine that will reduce all three pollutants. Catalytic

Table 3.3 SCR NO$_x$ catalyst technologies [57].

Company	Catalyst description	Operation temperature (^{0}C)
Babcock Hitachi	V/Ti/Metal plate	240-415
Camet	Precious metal/Metal monolith	225-275
Cormetech	V/Ti/Extruded monolith	200-450
Engelhard	Precious metal/Ceramic monolith	175-320
	V/Ti/Ceramic monolith	300-440
	Zeolite/Ceramic monolith	440-590
Hitachi Zosen	V/Ti/Extruded monolith	330-420
	V/Ti/Wire mesh	330-420
IHI	V/Ti/Extruded monolith	200-400
JMI	V/Ti/Metal monolith	340-425
KHI	V/Ti/Extruded monolith	300-400
MHI	V/Ti/Extruded monolith	200-400
Norton	Zeolite/Extruded monolith	220-520
Steuler	Zeolite/Extruded monolth	300-520
UBE	V/Ti/Extruded monolith	250-400

technology already exists that uses Pt and Pd for the abatement of CO and HC from a lean environment. A catalyst that can decompose NO_x to the equation below would represent the ideal solution [57] :

$$NO_x \longrightarrow N_2 + O_2 \qquad (3.20)$$
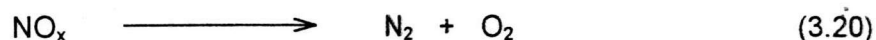
It could be installed in the exhaust gas as a passive device, requiring no major engine modifications. A less attractive but feasible fallback approach is to catalytically reduce the NO_x using on-board hydrocarbon (HC) [57].

$$HC + NO_x + O_2 \longrightarrow N_2 + H_2O + CO_2 \qquad (3.21)$$
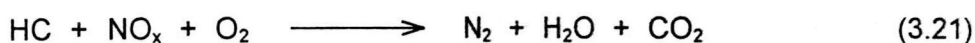
The technology requirements for this approach extend beyond catalyst materials, given that engine manufactureres must address the issue of providing sufficient hydrocarbons to react with the NO_x. In other words, a system solution must be found.

The catalyst must function under lean exhaust conditions. However, the biggest challenge for the catalyst is low-temperature operation for gasoline fueled vehicles and diesel passenger cars. Both require reductions of CO, HC, and NO_x below 200°C when located in the under-floor position. The diesel car has the additional requirement of particulate reductions [57]. A modification of existing oxidation catalyst/engine technology is being used to address the CO, HC, and particulates (diesel applications). No satisfactory solution currently exists for the NO_x. Catalyst formulation containing Pt is the most active for NO_x reduction between 180 and 300°C. Figure 3.21 plots NO_x reduction versus
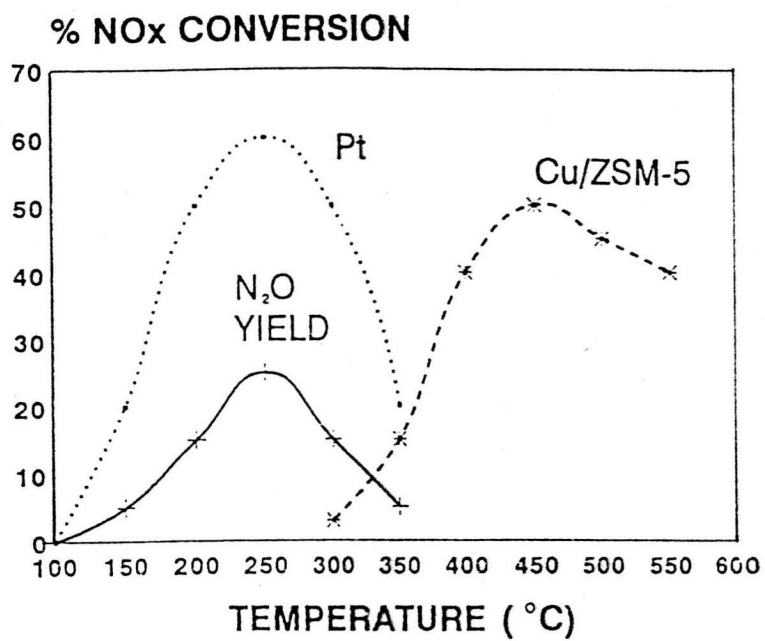
Figure 3.21 Lean NO_x conversion with propylene for a Pt and a Cu/ZSM-5

catalyst. Large yields of N_2O are generated with a Pt catalyst.

Cu/ZSM-5 converts the NO_x to N_2 [57].

temperature using olefin as a model compound for hydrocarbon reduction in engine exhaust [57]. The figure shows substantial formation of N_2O, which is a powerful greenhouse gas and may lead to ozone depletion in the upper atmosphere. Beyond about $300^{\circ}C$, the curve reaches a maximum, and the NO_x conversion quickly drops to zero.

Catalysts based on Cu/ZSM-5 are active at temperatures above about $300^{\circ}C$ but show the same type of selectivity behavior as Pt above about $400^{\circ}C$ [57]. Fortunately, little N_2O is formed. At higher temperature, the product is only N_2. Further increase in the HC-to-NO_x ratio results in small increase in the maximum NO_x conversion because most of the additional hydrocarbon is combusted, which makes the process less selective with increase HC to NO_x.

Lean-burn engines will have HC-to-NO_x ratios (C_1/NO_x mole basis) well below 1, making the reduction reaction very unfavorable because of the poor hydrocarbon selectivity for NO_x. Diesel engines already are lean-burn, and their gaseous C_1-to-NO_x mole ratios are below 0.1. So even if catalysts with close to 100 percent selectivity can be developed, there is insufficient hydrocarbon in the exhaust [57]. This is ironic, since engine manufactureres have modified their engines to reduce the hydrocarbons. This result is an undesirable fuel penalty but, with the proper engine injection control, a viable and cost-effective system can be developed.

3.7 X-ray Powder Diffraction

The first step in characterization of the solid isolated from the synthesis mixture is X-ray powder diffraction. The most significant information obtained about the solid is obtained from the diffraction pattern. This includes [40] :

1. Successful (or unsuccessful) formation of a crystalline material.

2. Presence of a single phase or mixture of phases.

3. With the presence of sufficient peaks, the identification of the structure type or structure types comprising the mixture.

4. If standards are available, the level of crystallinity obtained from that synthesis batch.

5. Ultimately, with the proper techniques, determination of a new structure.

The X-ray powder diffraction pattern of the solid obtained from the zeolite synthesis mixture is generally taken between the values of 5 °2θ and 40 °2θ. It is within this range that the most intense peaks characteristic of the zeolite structure occur. The peaks at values higher than 40 °2θ are of significantly low intensity, and, depending on the level of crystallinity, may not be observable. Therefore, for most routine X-ray identification of zeolite phases, the range between 5 and 40 °2θ is examined [40].

A common occurrence in zeolite synthesis is the presence of a noncrystalline product from a given reaction mixture. An example of an X-ray diffraction pattern for a typical unsuccessful synthesis is shown in Figure 3.22 (a). Beside the noncrystalline products possible form a give reactive mixture, crystalline but non-zeolite material may be obtained. The commonly observed crystalline phase obtained from an unsuccessful synthesis of the high-silica zeolites, for example, is cristobalite, a dense quartz phase. The cristobalite phase is a simple pattern to recognize, as it contains only one very intense line, between 5 °2θ and 40 °2θ. A typical X-ray trace of cristobalite is shown in
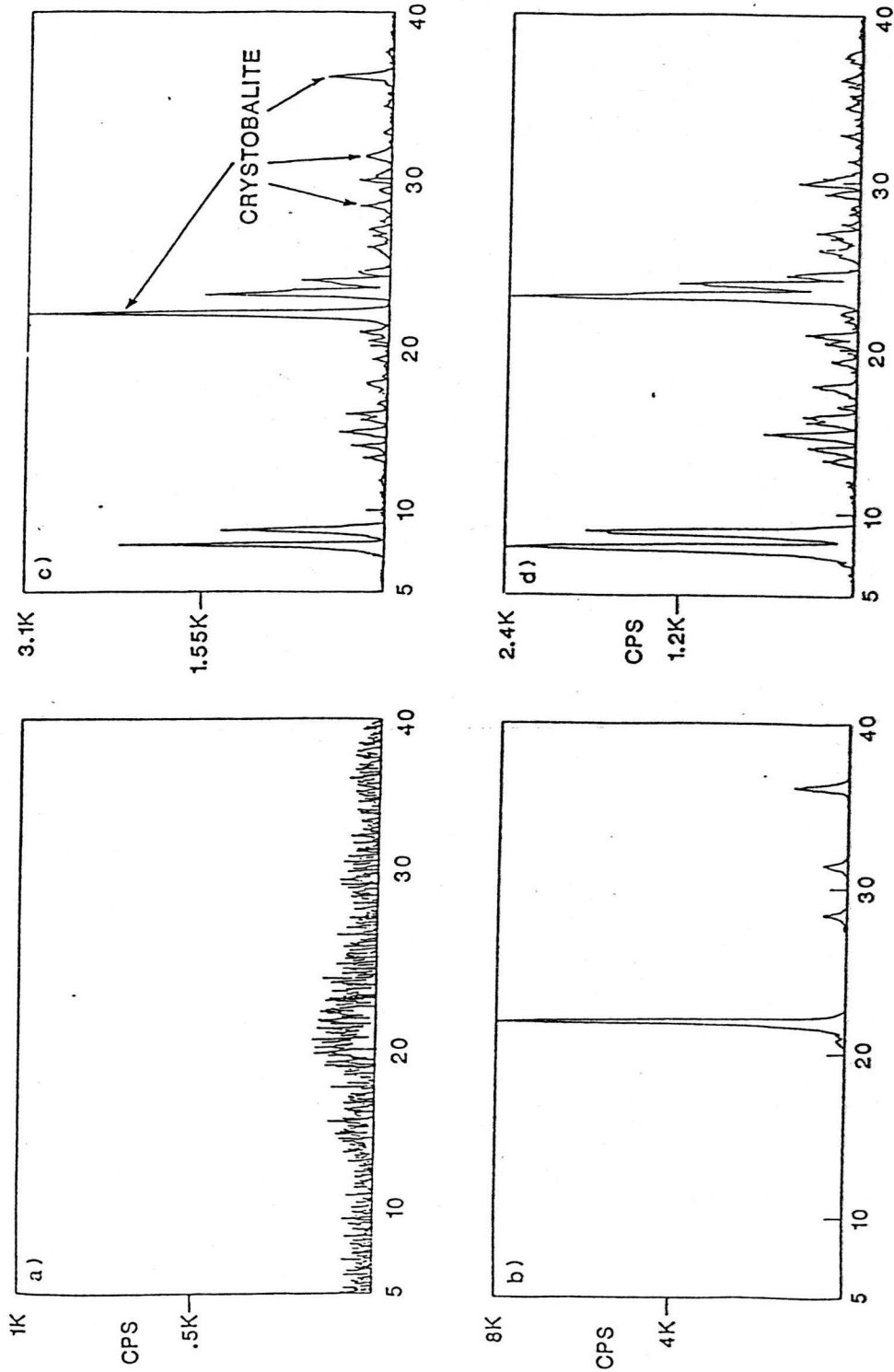
Figure 3.22 X-ray powder diffraction used to identify phase in synthesis of Zeolites[40].
a) Noncrystalline product b) crystalline but non-zeolitic phase (cristobalite shown in this example)
c) mixture of phase (crystobalite and ZSM-5)   d) pure single crystalline phase (ZSM-5)

Figure 3.22(b). In some systems, mixtures are obtained. These can be readily identified if individual X-ray diffraction patterns of all components are already known. For example, in Figure 3.22(c), a mixture of cristobalite and ZSM-5 was produced from the reaction mixture. As both components are already well known, a comparison of these values with standard literature values for the X-ray diffraction patterns of cristobalite and ZSM-5 will confirm these components of the mixture. By changing the synthesis parameters, the zeolite phase can (in many cases) be optimized and the second phase suppressed, as shown in Figure 3.22(d). Here a sharp pattern for a well-crystallized ZSM-5 sample was obtained.

Many times in exploratory zeolite synthesis aimed at producing new structures, material are obtained with X-ray patterns that appear to indicate a single phase and are already related in peak position to a known structure. However, in some cases the peak intensities are not in agreement. Changes in relative peak intensity have been occurred [40]:

1. Upon removal of an organic additive from the pores or changing the cations within the pores of the higher-silica-contain materials.

2. Upon changing the counter-ion.

3. When large crystals have a preferred orientation in the X-ray sample holder.

4. When other ions are substituted into the framework structure.